Modeling and Experiment on Active Magnetic Bearing as Force Actuators to Detect Inner Race Fault of Rolling Element Bearing

Yuanping Xu, Jin Zhou, and Chaowu Jin

College of Mechanical and Electrical Engineering
Nanjing University of Aeronautics and Astronautics, Nanjing, 210016, China
ypxu@nuaa.edu.cn, zhj@nuaa.edu.cn, jinchaowu@nuaa.edu.cn

Abstract ─ As one of the important components in the rotating machinery, the condition of rolling element bearing has a great impact on the system performance. Therefore, the fault detection for the rolling element bearing is important and many methods have been proposed. Following our previous work on the outer race defect diagnosis, in this paper, the active magnetic bearing (AMB) is employed as an exciter to apply electromagnetic force to detect the inner race defects. The theoretical model of a nonlinear bearing-pedestal system model with the inner race defect under the electromagnetic force is developed and investigated. The simulation and experimental results show that the characteristic signal of inner race defect is amplified under the electromagnetic force through the AMBs, which is helpful for improving the diagnosis accuracy.

Index Terms ─ Active magnetic bearings, fault detection, inner race, rolling element bearings.

I. INTRODUCTION

For the rotating machinery, the health condition of rolling element bearing has a great impact on the performances. Therefore, fault detection for the rolling element bearing is very important and many methods have been proposed, which can be classified as vibration measurement, acoustic measurement, temperature measurement and wear analysis [1]. Vibration measurement has been the most widely used method in the health monitoring application.

A lot of methods have been proposed to model the vibration response of a bearing. McFadden and Smith [2,3] proposed a theoretical defected rolling element bearing model. Wang and Harrap [4] presented the envelope autocorrelation analysis for diagnosing multiple element defects of rolling element bearings. Tandon and Choudhury [5] investigated the dynamic response of the rings due to localized defects under axial load. Sunnersjo [6] proposed a two degrees of freedom (DOF) bearing dynamic model and applied Hertz contact theory to calculate the deflection. Feng [7] developed a four DOF bearing-pedestal model, which include two DOF pedestal model. Tadina [8] developed an improved bearing model and investigated the vibrations of a rolling element bearing during run-up.

AMBs are commonly used as bearings to support rotor, but they also can be used for fault detection as exciters [9]. Humphris [10] utilized AMBs as both levitation and perturbation to monitor and diagnose the shaft condition. Zhu et al. [11] modeled a crack rotor levitated by AMBs and found that crack would have big effects on the whole system. Mani et al. [12,14] and Quinn et al. [13] applied excitation from the AMB to a cracked rotor bearing system and used multiple scale method to diagnose the rotor crack. Similarly, Sawicki [15] applied harmonic balance method based on sinusoidal excitation generated from AMBs for rotor crack detection. Chasalevris [16] investigated the response of a simple elastic rotor supported by two fluid-film bearings, while one of the bearings was worn under the AMB transient excitation.

Although AMBs have been used for the fault detection, few studies are reported on rolling element bearings. In our previous work [17], the AMB is employed as an exciter to detect the outer race defects and we found that the outer race fault signals amplified significantly under AMBs force. Following our previous work on the outer race defect, this paper investigates dynamic response of inner race defect under electromagnetic force excitation.

The remainder of the paper is organized as follows. Section 2 describes the model of rolling element bearing system with inner race defect under AMB force. The simulation and experimental results are presented in Section 3 and Section 4, respectively. Conclusions are drawn in Section 5.

II. ROLLING ELEMENT BEARING MODELING

A. Contact force

Figure 1 shows the bearing schematic, where N is number of rolling elements; d_b is the element diameter; D is the pitch diameter; r_0 is the radial clearance; α

Submitted On: May 22, 2018
Accepted On: October 4, 2018

is and the contact angle. The bearing is modeled with two orthogonal DOF and the outer race is fixed in the pedestal. The slippage of rolling elements, the mass and the inertia of the rolling elements are ignored. The displacement of the shaft can be divided into x and y directions and the contact deformation for the ith rolling element δ_i is given by:

$$\delta_i = x\cos\theta_i + y\sin\theta_i - r_0. \tag{1}$$

The angle of the rolling element θ_i shown in Fig. 1 is given as:

$$\theta_i = \omega_c t + \frac{2\pi}{N}(i-1), \tag{2}$$

$$\omega_c = \frac{\omega_s r}{(R+r)}, \tag{3}$$

where ω_s is the shaft speed; ω_c is the cage speed; r and R in Fig. 1 are the inner and outer race radius.

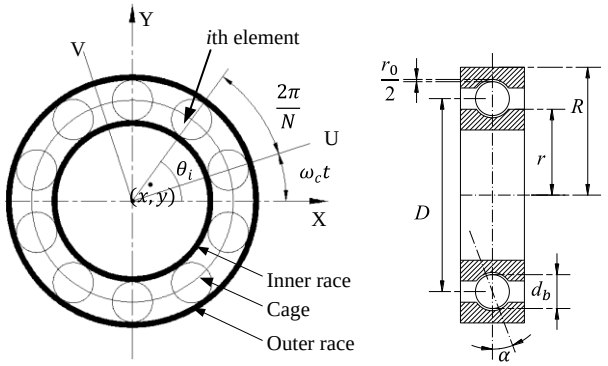

Fig. 1. Schematic of a rolling element bearing.

According to the Hertz theory, the non-linear contact force F is given by [1,18-19]:

$$F = K_b\delta^n, \tag{4}$$

where δ is the contact deformation; K_b is the nonlinear contact stiffness depending on the bearing geometry and the elasticity of material [18], for the rolling element bearing considered in this paper, the computed value is 2.14×10^9 N/m$^{1.5}$; the exponent $n = 1.5$ is for ball bearings. Due to the fact that compression Hertz forces occurs only for positive values of δ, therefore the γ_i is employed to represents the contact state:

$$\gamma_i = \begin{cases} 1 & \text{if } \delta_i > 0 \\ 0 & \text{if } \delta_i \le 0 \end{cases}. \tag{5}$$

The contact force is the sum of each of the rolling elements and the total force along the x and y axes can be obtained as:

$$F_{bx} = \sum_{i=1}^{N}\gamma_i K_b\delta_i^{1.5}\cos\theta_i, \tag{6}$$

$$F_{by} = \sum_{i=1}^{N}\gamma_i K_b\delta_i^{1.5}\sin\theta_i. \tag{7}$$

The damping of rolling element bearing can be estimated using Kramer method [20] as:

$$c_s = (0.25-2.5)\times10^{-11}K_l, \tag{8}$$

where K_l is the linearized stiffness of the rolling element bearing.

B. Inner race defect modeling

The inner race defect is modeled as a slight dent and the geometrical interpretation of the faults is shown in Fig. 2.

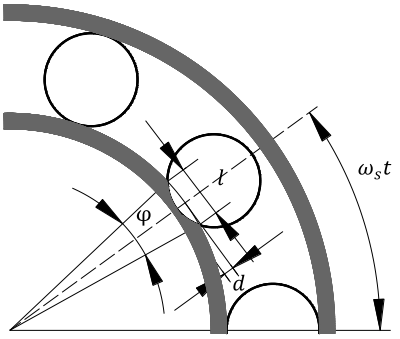

Fig. 2. Defect on inner race.

The length of the dent is l and the following relationship can be established from Fig. 2:

$$d = r_b - \sqrt{r_b^2 - (l/2)^2}, \tag{9}$$

$$\varphi = 2\sin^{-1}(l/2r), \tag{10}$$

where r_b is the ball radius; φ is the central angle of the inner defect; d is the max increment of the radial clearance.

When the rolling element moves into the defected area, the radial clearance will increase rapidly, which causes a decline of the contact force and results vibration. The varying clearance Δd caused by the defect is modeled as a half sinusoidal wave [17]. The relation between the varying clearance and angular position is give as follows:

$$\Delta d(\theta_i) = \begin{cases} d\sin\left[\pi\dfrac{\bmod(\theta_i,2\pi)-\left(\omega_s t-\dfrac{\varphi}{2}\right)}{\varphi}\right], & \bmod\left(\omega_s t-\dfrac{\varphi}{2},2\pi\right) < \bmod(\theta_i,2\pi) < \bmod\left(\omega_s t+\dfrac{\varphi}{2},2\pi\right) \\ 0, & \text{otherwise} \end{cases}. \tag{11}$$

The notation $\mathrm{mod}(\theta_i,2\pi)$ in Eq. (11) denotes the modulo operation. From Eq. (9), the $\Delta d(\theta_i)$ value range is 0 to 3×10^{-3} mm considering l as 0.2 mm.

Therefore, when the rolling element is not located in the defected region, the actual radial clearance r_a is:

$$r_a = r_0. \tag{12}$$

When the rolling element is located in the defected region, the actual radial clearance r_a is:

$$r_a = r_0 + \Delta d. \tag{13}$$

Therefore, the contact forces can be calculated as follows:

$$F_{bx} = \sum_{i=1}^{N} \gamma_i K_b \left(x\cos\theta_i + y\sin\theta_i - r_a\right)^{1.5} \cos\theta_i, \tag{14}$$

$$F_{by} = \sum_{i=1}^{N} \gamma_i K_b \left(x\cos\theta_i + y\sin\theta_i - r_a\right)^{1.5} \sin\theta_i. \tag{15}$$

B. Bearing-pedestal modeling

The model of Feng et al. [7] is adopted to study the dynamics of rolling element bearings, which is shown in Fig. 3. The model has four DOF, including two DOF of inner race (x_s, y_s) and two DOF of pedestal (x_p, y_p).

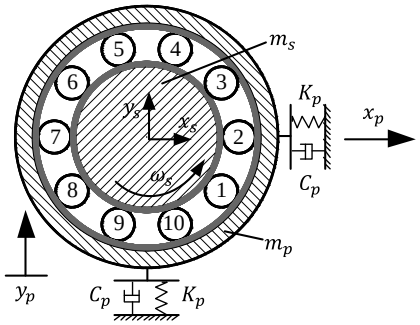

Fig. 3. Four-DOF bearing-pedestal model.

Followed by the above analysis, the whole contact forces of the model considering inner race and pedestal can be calculated as follows:

$$F_{bx} = \sum_{i=1}^{N} \gamma_i K_b \left[\left(x_s - x_p\right)\cos\theta_i + \left(y_s - y_p\right)\sin\theta_i - r_a\right]^{1.5} \cos\theta_i, \tag{16}$$

$$F_{by} = \sum_{i=1}^{N} \gamma_i K_b \left[\left(x_s - x_p\right)\cos\theta_i + \left(y_s - y_p\right)\sin\theta_i - r_a\right]^{1.5} \sin\theta_i. \tag{17}$$

Considering the nonlinear contact force, the equations of motion of bearing-pedestal system can be written as follows:

$$m_s\ddot{x}_s + c_s\dot{x}_s + F_{bx} = F_u\cos\omega_s t + F_{MX}, \tag{18}$$

$$m_s\ddot{y}_s + c_s\dot{y}_s + F_{by} = F_u\sin\omega_s t - m_s g + F_{MY}, \tag{19}$$

$$m_p\ddot{x}_p + c_p\dot{x}_p + K_p x_p - F_{bx} = 0, \tag{20}$$

$$m_p\ddot{y}_p + c_p\dot{y}_p + K_p y_p - F_{by} = -m_p g, \tag{21}$$

where m_s is the mass of the shaft and the inner race; c_s is the bearing damping; m_p is the mass of the pedestal; K_p and c_p are the stiffness and damping of the pedestal. F_{MX} and F_{MY} is the electromagnetic force applied to the system in the x and y direction, respectively, which are presented later. F_u is the unbalance force.

C. AMB force modeling

Ignoring the hysteresis loss and eddy current effect, the electromagnetic force provided by AMBs can be calculated by [21]:

$$F_{AMB} = \frac{1}{4}\mu_0 n_a^2 A\frac{i^2}{s^2}\cos\beta, \tag{22}$$

where μ_0 is the permeability in the vacuum; n_a is the number of coil windings; A is the area of the pole face; i is the bias current value; s is the nominal air gap and β is the angle between forces and magnetic poles. Table 1 lists the AMB parameters. Figure 4 shows the schematic of the AMB structure adopted in this paper, which the bottom two poles are activated.

Table 1: AMB parameters

Air Gap (AMB clearance) s	0.28 mm
Polar face area A	2.0×10^{-4}m^2
Windings of a coil n_a	240
Half angle between two poles β	22.5 degree

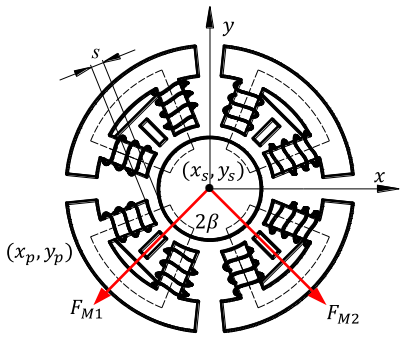

Fig. 4. The schematic of the AMB structure.

When the rolling element is located at the defected region, the rotor and the pedestal will vibrate and the nominal air gap s between the rotor and AMBs will change simultaneously since the AMBs are fixed on the stator together with the pedestal. Therefore, the electromagnetic force of each AMB can be written as:

$$F_{M1} = \frac{\mu_0 n_a^2 A i^2\cos\beta}{4\left[s + \left(y_s - y_p\right)\cos 2\beta + \left(x_s - x_p\right)\sin 2\beta\right]^2}, \tag{23}$$

$$F_{M2} = \frac{\mu_0 n_a^2 A i^2\cos\beta}{4\left[s + \left(y_s - y_p\right)\cos 2\beta + \left(x_p - x_s\right)\sin 2\beta\right]^2}. \tag{24}$$

Therefore, the total electromagnetic force along the x and y directions is:

$$F_{MX} = -\left(F_{M1}\sin 2\beta - F_{M2}\sin 2\beta\right), \quad (25)$$

$$F_{MY} = -\left(F_{M1}\cos 2\beta + F_{M2}\cos 2\beta\right). \quad (26)$$

III.SIMULATION RESULTS

A. Model parameters

The nonlinear differential Eq. (18-21) is evaluated numerically using the fourth-order Runge-Kutta algorithm and the transient response is obtained. The parameters adopted in simulation are shown in Table 2.

Table 2: Model parameters

1. Parameters of 61901 Rolling Element Bearings	
Outer race radius R	10.59 mm
Inner race radius r	7.41 mm
Number of ball N	10
Contact stiffness K_b	2.14×10^9 N/m$^{3/2}$
Ball diameter d_b	3.18 mm
Pitch diameter D	18 mm
Contact angle α	0°
Radial clearance r_0	3 μm
B_N	4.1
2. Other Inputs	
Mass of shaft/inner race m_s	1.2 kg
Bearing contact damping c_s	200 N · s/m
Mass of pedestal m_p	2 kg
Pedestal stiffness K_p	1.5×10^7 N/m
Damping in pedestal c_p	3000 N · s/m
Bias current i	1 A

The vertical acceleration responses for the pedestal with an inner racer faulty bearing are calculated respectively considering the electromagnetic force is applied or not. The frequency spectrum of the vibration signal is obtained using envelope method rather than the Fast Fourier Transform Algorithm (FFT) directly because in most cases, these defect frequencies cannot be detected in the frequency spectrum of a raw vibration signal due to the dominant high frequencies caused by the resonant components.

B. Inner race defect under electromagnetic force

For a rolling element bearing, the inner race defect frequency is given by [1]:

$$f_{BPFI} = \frac{1}{2} f_s \left(1 + \frac{d_b}{D}\cos\alpha\right) N, \quad (27)$$

where f_s is the shaft rotating speed in Hz.

The defect on the inner race will rotate along the shaft haft rotating speed and will go through the loading zone every cycle. Thus the peaks at BPFI (Ball Pass Frequency Inner), the combination of the BPFI with inner ring (shaft frequency) will be found in the frequency domain. Figures 5 (a) and (b) show the simulated vertical pedestal acceleration in time domain due to inner race defect with and without electromagnetic force. It is clear that the vibration amplitudes aggravate obviously under the electromagnetic force. The envelope spectrum (Hilbert transform) for the time domain in Fig. 5 (c) shows a frequency peak at 30 Hz, which is the rotating frequency. The theoretical inner race defect frequency BPFI calculated by Eq. (27) is 176.5 Hz which equals to the simulation value, indicating the model is accurate. It can be seen from the Fig. 5 (c) that for a small defect, the amplitude of defect characteristic frequency BPFI and the combination of the BPFI with inner ring rotating frequency are small in the frequency spectrum. However, there is clear increase for these peaks under the electromagnetic force. This may be attributed to the electromagnetic force property, which changes periodically due to the periodically changing of the air gap. In other words, when the rolling elements locate at the defected area, the rotor will vibrate, causing a varying air gap and leading to the same periodically varying electromagnetic force. Because the electromagnetic force varying frequency equals to the inner race defect characteristic frequency f_{BPFI}, the f_{BPFI} characteristic signal will be amplified clearly.

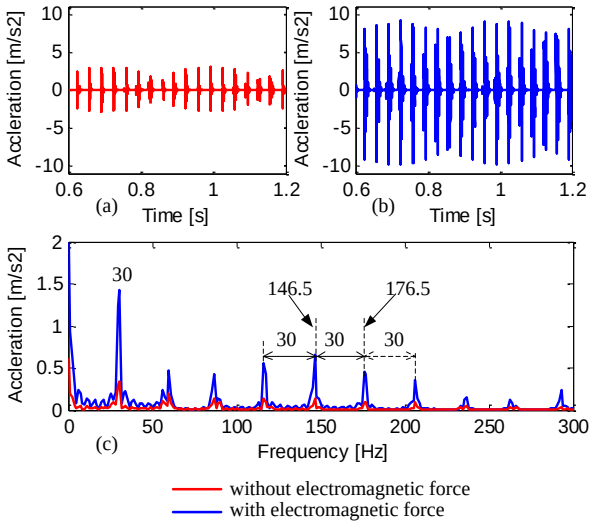

Fig. 5. Simulated pedestal vertical vibration with bearing inner race defect, $l = 0.2$mm, at 1800 rpm (30 Hz): (a) bearing without electromagnetic force, (b) bearing with electromagnetic force, and (c) frequency spectrum of the envelope between 0.6 and 1.2s.

IV. EXPERIMENTAL INVESTIGATION

The experimental test rig for this study is a rotor AMB system designed and built as a research platform at Nanjing University of Aeronautics and Astronautics, as shown in Fig. 6. The rotor was supported by two radial and two thrust AMBs. However, for this study, the

system is rearranged that the rotor is supported by rolling element bearings rather than AMBs and the AMBs are employed as the non-contact exciters to apply online electromagnetic force during the operation. One acceleration sensor is installed on the pedestal vertically to record the acceleration vibration data.

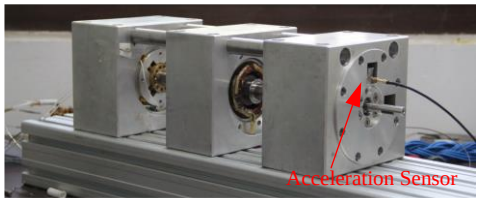

Fig. 6. The test rig.

Fig. 7. The damage process using electric discharge machine.

Figure 7 shows inner race damage process using electric discharge machine. The width of this damage is around 0.2 mm.

The experiment is performed at 1800 rpm (30 Hz) under radial AMB force with 1A bias current. Figure 8 shows the experimental results. Figures 8 (a) and 8 (b) are the time domain acceleration signal with and without AMBs, respectively. Corresponding envelope frequency spectrum (Hilbert transform) comparisons for the faulty inner race bearing are shown in Fig. 8 (c) and Fig. 8 (d). It can be seen that for an incipient defect, when electromagnetic force is not applied, the vibration amplitudes in the time domain, the peaks of f_{BPFI} and the combination of the BPFI with inner ring in frequency spectrum are small. However, there is clear increase in peaks at peaks of f_{BPFI} and the combination of the BPFI with inner ring under electromagnetic force. The experimental peak frequency of f_{BPFI} is 177.7 Hz, which almost coincides with the simulation results (176.5 Hz) and the theoretical calculation from Eq. (27). Both experimental and simulation results show an increase in the acceleration response as a result of the defect in the inner race.

V. CONCLUSION

The health condition of rolling element bearing has a great impact on the rotating machinery performances. In this paper, the dynamics of an inner race fault rolling element bearing with AMBs as force actuators is studied. We investigate a nonlinear bearing pedestal model with the inner race defect under the electromagnetic force and obtain the numerical simulation results. The results show that under the electromagnetic force generated from AMBs, the peaks of f_{BPFI} and the combination of the BPFI with inner ring in frequency spectrum for the inner race are amplified clearly, which is helpful for improving the diagnosis accuracy. In order to verify our theoretical calculation, an experiment is performed, which validate theoretical results.

Since the single defect model with AMBs excitation is validated, we think this model may also be available for multiple defects. In the future, the multiple defects condition and sensitivity of this method will be investigated.

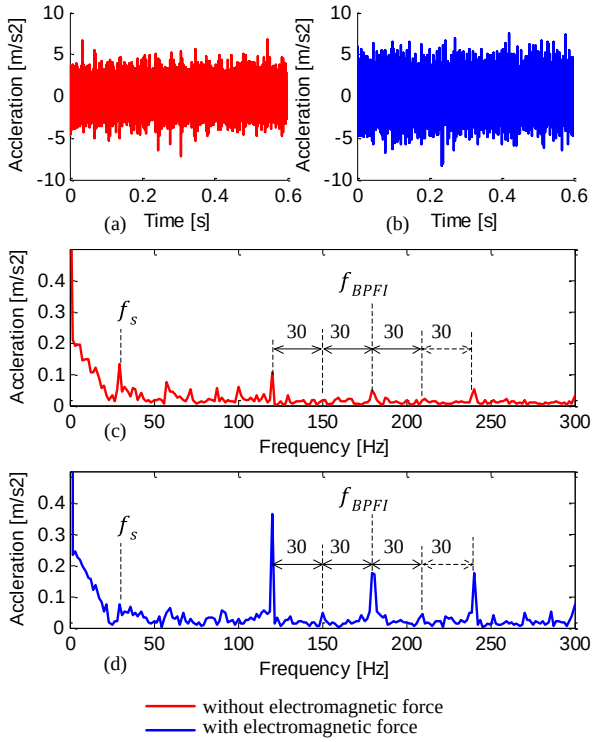

Fig. 8. Experimental pedestal vertical vibration with bearing inner race defect, $l = 0.2\mathrm{mm}$, at 1800 rpm (30 Hz): (a) bearing without electromagnetic force, (b) bearing with electromagnetic force, (c) the envelope frequency spectrum for a, and (d) the envelope frequency spectrum for b.

ACKNOWLEDGMENT

This work is supported by Open Project Program of Jiangsu Key Laboratory of Large Engineering Equipment Detection and Control (JSKLEDC201502).

REFERENCES

[1] M. S. Patil, J. Mathew, P. K. Rajendrakumar, and S. Desai, "A theoretical model to predict the effect of localized defect on vibrations associated with ball bearing," *International J. Mechanical Sciences*, vol. 52, no. 9, pp. 1193-1201, 2010.

[2] P. D. McFadden and J. D. Smith, "Model for the vibration produced by a single point defect in a rolling element bearing," *J. Sound and Vibration*, vol. 96, no. 1, pp. 69-82, 1984.

[3] P. D. McFadden and J. D. Smith, "The vibration produced by multiple point defects in a rolling element bearing," *J. Sound and Vibration*, vol. 98, no. 2, pp. 263-273, 1985.

[4] W. Y. Wang and M. J. Harrap, "Condition monitoring of ball bearings using an envelope autocorrelation technique," *Machine Vibration*, vol. 5, no. 1, pp. 34-44, 1996.

[5] N. Tandon and A. Choudhury, "An analytical model for the prediction of the vibration response of rolling element bearings due to a localized defect," *J. Sound and Vibration*, vol. 205, no. 3, pp. 275-292, 1997.

[6] C. S. Sunnersjö, "Varying compliance vibrations of rolling bearings," *J. Sound and Vibration*, vol. 58, no. 3, pp. 363-373, 1978.

[7] N. S. Feng, E. J. Hahn, and R. B. Randall, "Using transient analysis software to simulate vibration signals due to rolling element bearing defects," *The 3rd Australian Congress on Applied Mechanics*, Sydney, pp. 689-694. 2002.

[8] M. Tadina and M. Boltežar, "Improved model of a ball bearing for the simulation of vibration signals due to faults during run-up," *J. Sound and Vibration*, vol. 330, no. 17, pp. 4287-4301, 2011.

[9] J. T. Marshall, M. Kasarda, and J. Imlach, "A multipoint measurement technique for the enhancement of force measurement with active magnetic bearings," *J. Engineering for Gas Turbines and Ppower*, vol. 125, no. 1, pp. 90-94, 2003.

[10] R. R. Humphris, "A device for generating diagnostic information for rotating machinery using magnetic bearings," *The MAG Conference & Exhibition for Magnetic Bearings, Magnetic Drives and Dry Gas Seals*, 1992.

[11] C. Zhu, D. A. Robb, and D. J. Ewins, "The dynamics of a cracked rotor with an active magnetic bearing," *J. Sound and Vibration*, vol. 265, no. 3, pp. 469-487, 2003.

[12] G. Mani, D. D Quinn, M. Kasarda, D. J. Inman, and R. G. Kirk, "Health monitoring of rotating machinery through external forcing," *Proceedings of ISCORMA-3*, Cleveland, USA, pp. 19-23, 2005.

[13] D. D Quinn, G. Mani, M. Kasarda, T. Bash, D. J. Inman, and R. G. Kirk, "Damage detection of a rotating cracked shaft using an active magnetic bearing as a force actuator—Analysis and experimental verification," *IEEE/ASME Trans. Mechatronics*, vol. 10, no. 6, pp. 640-647, 2005.

[14] G. Mani, D. D Quinn, and M. Kasarda, "Active health monitoring in a rotating cracked shaft using active magnetic bearings as force actuators," *J Sound and Vibration*, vol. 294, no. 3, pp. 454-465, 2006.

[15] J. T. Sawicki, M. I. Friswell, Z. Kulesza, A. Wroblewsk, and J. D. Lekki. "Detecting cracked rotors using auxiliary harmonic excitation," *J. Sound and Vibration*, vol. 330, no. 7, pp. 1365-1381, 2011.

[16] A. Chasalevris, F. Dohnal, and I. Chatzisavvas, "Experimental detection of additional harmonics due to wear in journal bearings using excitation from a magnetic bearing," *Tribology International*, vol. 71, pp. 158-167, 2014.

[17] Y. Xu, L. Di, J. Zhou, C. Jin, and Q. Guo, "Active magnetic bearings used as exciters for rolling element bearing outer race defect diagnosis," *ISA Transactions*, vol. 61, pp. 221-228, 2016.

[18] J. Sopanen and A. Mikkola, "Dynamic model of a deep-groove ball bearing including localized and distributed defects, Part 1: Theory," *Proceedings of the Institution of Mechanical Engineers, Part K: J. Multi-body Dynamics*, vol. 217, no. 3, pp. 201-211, 2003.

[19] N. Sawalhi and R. B. Randall, "Simulating gear and bearing interactions in the presence of faults: Part I. The combined gear bearing dynamic model and the simulation of localised bearing faults," *Mechanical Systems and Signal Processing*, vol. 22, no. 8, pp. 1924-1951, 2008.

[20] E. Kramer. *Dynamics of Rotors and Foundations*. Berlin: Springer-Verlag, 1993.

[21] G. Schweitzer and E. H. Maslen, *Magnetic Bearings*. Springer, Berlin, Germany, 2009.

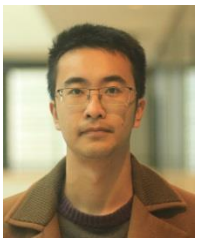

Yuanping Xu received his Ph.D. degree in Mechanical Engineering from Nanjing University of Aeronautics and Astronautics (NUAA) in 2018. From 2016 to 2017, he was a Guest Ph.D. Student in Ecole Polytechnique Federale Lausanne (EPFL), Switzerland. He is currently a Lecturer in the College of Mechanical and Electrical Engineering, NUAA. His research focuses on magnetic levitation.

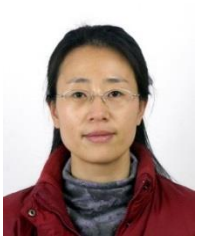

Jin Zhou received her Ph.D. degree in Mechanical Engineering from China University of Mining and Technology (CUMT) in 2001. From 2012 to 2013, she was a visiting scholar in the Rotating Machinery and Control Laboratory (ROMAC) of the University of Virginia. She is currently a Full Professor in the College of Mechanical and Electrical Engineering, NUAA. Her research focuses on magnetic bearings and vibration control. She was the member of Program Committee of the 14th International Symposium on Magnetic Bearings (2014) and the Program Chair of the 16th International Symposium on Magnetic Bearings, 2018.

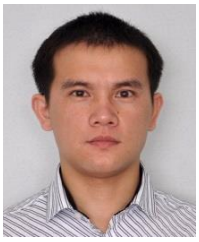

Chaowu Jin obtained the B.S., M.S., and Ph.D. degree in Mechanical Engineering from NUAA from 2002 to 2011. He is currently an Associate Professor in the College of Mechanical and Electrical Engineering, NUAA. His research focuses on magnetic bearings.